Journal of Advanced Research in Applied Sciences and Engineering Technology

Journal homepage:
https://semarakilmu.com.my/journals/index.php/applied_sciences_eng_tech/index
ISSN: 2462-1943

Influence of Parasitic Elements on Flyback Converter at High Switching Frequency Operation: A Comprehensive Analysis

Muhamad Faizal Yaakub[1,2,*], Mohd Amran Mohd Radzi[2], Faridah Hanim Mohd Noh[3], Norhafiz Azis[2], Ahmed Naji Zaidan[2,4]

1 Fakulti Teknologi dan Kejuruteraan Elektrik, Universiti Teknikal Malaysia Melaka, Hang Tuah Jaya, 76100 Durian Tunggal, Melaka, Malaysia
2 Advanced Lightning, Power and Energy Research Centre, Department of Electrical and Electronic Engineering, Faculty of Engineering, Universiti Putra Malaysia, 43400 Serdang, Selangor, Malaysia
3 Department of Electrical Engineering Technology, Faculty of Engineering Technology, Universiti Tun Hussein Onn Malaysia, Parit Raja, 86400 Batu Pahat, Johor, Malaysia
4 College of Engineering, Al-Iraqia University, Baghdad Governorate, Iraq

ABSTRACT

The presence of parasitic elements in the flyback converter amplifies the impact on the converter’s primary current quality, particularly when the converter's switching frequency exceeds its designated operational rate. In this paper, the parasitic and stray elements of the transformer have been comprehensively examined, modelled, and simulated to evaluate their influence on the converter, with specific emphasis on the primary current. The simulation was performed utilising MATLAB SIMULINK software, integrating the authentic critical characteristics of the components, and conducting tests at various switching frequencies. The simulation results indicate that the primary current exhibits pronounced resonance effects at higher switching frequencies. The experimental findings are presented to corroborate the theoretical analysis and simulations pertaining to the impact of parasitic elements on the transformer and its immediate environment.

Keywords:
DC-DC converter; flyback; parasitic; primary current

1. Introduction

Flyback converters are one of the most basic, conventional power electronic circuits, with an isolated conversion of DC to DC at the minimal possible component count. The ongoing interest in the flyback converter stems mostly from the growing demand for renewable energy, such as solar photovoltaic (PV) applications and the rapid development of semiconductor devices [1-7]. A flyback converter has been widely employed in various single-stage and multi-stage PV micro-inverters due to its simplicity and remarkable performance in DC-DC step-up applications, including its excellent capacity for galvanic isolation [8,9].

* *Corresponding author.*
E-mail address: muhamadfaizal@utem.edu.my

https://doi.org/10.37934/araset.58.1.220230

The Flyback transformer-based converter continues to draw interest in several studies to increase its performance in a variety of ways, for instance, control algorithms [10], converter topologies [11], and the effect of parasitic elements in the transformer [12]. The impact of transformer parasitic is typically studied in terms of leakage inductance, especially in low voltage high current applications [13,14], where the influence of leakage inductance is more dominant. The stray capacitance, on the other hand, is more prominent in the overall influence of the transformer parasitic in high voltage low power applications as a result of the charging and discharging activity of the capacitors [15].

Despite the fact that there have been numerous research studies on the effect of parasitism in flyback converters, they have primarily focused on low switching frequency operation [16-19]. When used at high switching frequencies, in addition to the high transformation ratio, the parasitic presence in flyback transformers may significantly affect the converter's performance. This is correct when a peak current control is employed in boundary conduction mode (BCM) operation. In previous literature, the area at the corner end of the reference current was omitted to avoid further power losses at light load conditions. The switching frequency in this area is exceptionally high due to variable frequency operation in BCM. As a result, a distorted input primary current is induced, caused by the LC resonance circuit [20,21].

This article offers an analysis of the impact of parasitic elements on the flyback transformer, explicitly focusing on their influence on the input primary current utilised for current peak control operation. The analysis entails a comprehensive examination of the parameters of the flyback transformer, followed by the simulation of a modelled converter circuit using MATLAB SIMULINK software. The parameters utilised in the simulation are obtained through measurements conducted on the actual flyback transformer. Furthermore, this study examines the impact of switching frequencies on the behaviour of the transformer in relation to the presence of surrounding parasitic elements. The simulation reveals that primary current is added with significant resonance at high switching frequencies. Consequently, experimental results are provided to validate the theoretical analysis and simulations of the influence of parasitic elements on the transformer and its surroundings.

2. Flyback Transformer Equivalent Circuit

The equivalent circuit for a flyback transformer is thoroughly investigated. The investigation revealed that diverse applications and approaches would result in various transformer models [19,22-25]. The equivalent model is essential to this study because it will simulate parasitic elements' impact on converter behaviour. Figure 1 illustrates the 6C-model of the flyback transformer with its typical parasitic passive elements.

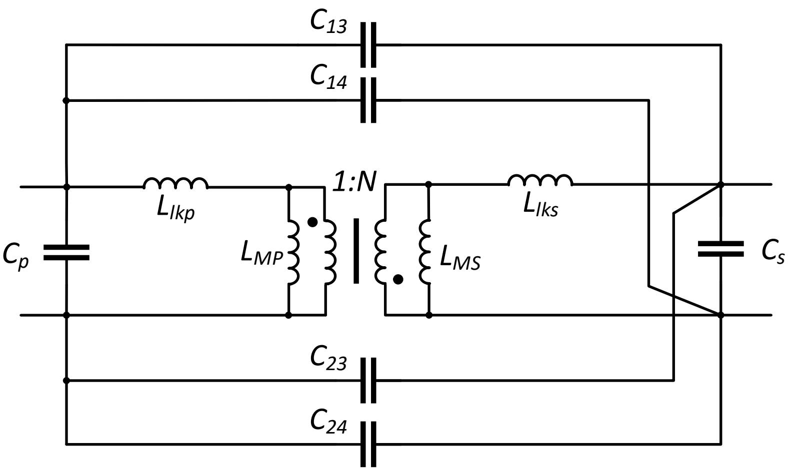

Fig. 1. Flyback transformer 6c-model equivalent circuit

This model is constructed from an electrostatic part of six capacitances and the magnetic part of leakage and magnetising inductance. However, the electrostatic part is irrelevant to the analysis of flyback converters and can be simplified to a single capacitor model [25]. From this model, the energy stored in the transformer can be deduced by:

$$E_T = \frac{1}{2} V_P^2 [C_P + C_S N^2 + C_{13}(N-1)^2 + C_{23} N^2 + C_{14}] \quad (1)$$

where C_p is the primary capacitance, C_s is the secondary capacitance, C_{13}, C_{14}, and C_{23} are the interwinding capacitance, and V_P is the input voltage's supply of the voltage across C_P. From Eq. (1), the simplified equivalent capacitance can be expressed as:

$$C_q = C_P + C_S N^2 + C_{13}(N-1)^2 + C_{23} N^2 + C_{14} \quad (2)$$

The dynamic conduct and capacitive energy observed from the primary and secondary input are thoroughly described through the equivalent capacitance C_q. Figure 2 shows the simplified model that will be used and simulated in MATLAB SIMULINK simulation software.

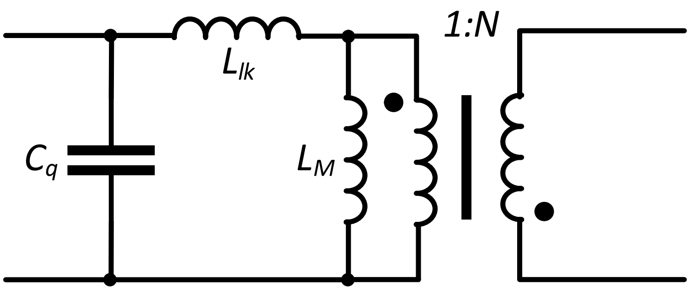

Fig. 2. Simplified equivalent circuit used in simulation

3. Operational Characteristic

3.1 Circuit Configuration

A typical flyback DC-DC converter circuit used in the microinverter is illustrated in Figure 3(a), ideally constructed by several key components such as a flyback transformer, power MOS switching device, fast recovery diode, and output capacitor. However, practically, there are non-ideal components such as transformer leakage inductance (L_{lkp}, L_{iks}), magnetising inductance (L_{MP}, L_{MS}), primary and secondary capacitance (C_P, C_S), interwinding capacitance (C_{12}) and other stray capacitance at the active components (C_{S_oss}, C_{D_oss}) that influence the operation of flyback converter, depending on the mode of operation and switching frequencies. The typical flyback circuit with parasitic elements is illustrated in Figure 3(b).

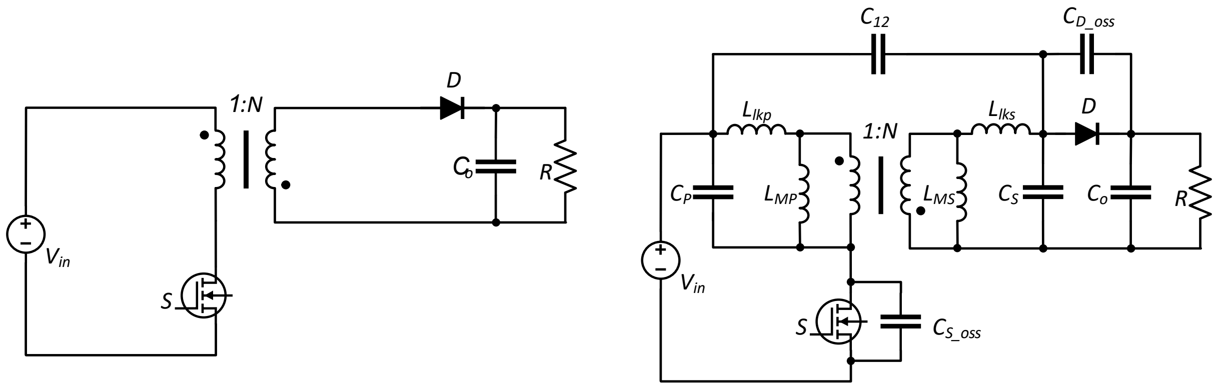

(a) (b)

Fig. 3. (a) Basic flyback converter circuit typically used in PV microinverter and (b) Common flyback converter with parasitic elements

3.2 Analysis of Operational Mode

Consequently, the circuit depicted in Figure 3 initiates the current response for a single switching cycle, as demonstrated in Figure 4, wherein it is divided into four distinct intervals. The magnetising current of the transformer is illustrated in dotted blue marked with $i_M(t)$; the ideal primary current of the converter is depicted with a solid green line marked with $i_p(t)$, while the dotted red marked with $i_p'(t)$ represents the primary current influenced by parasitic elements at high switching frequencies. Figure 5 depicts the circuits that represent each interval inside the switching cycle. The solid red line in the circuit diagram shows the primary current flow, while the dotted green line represents the current response at high frequencies.

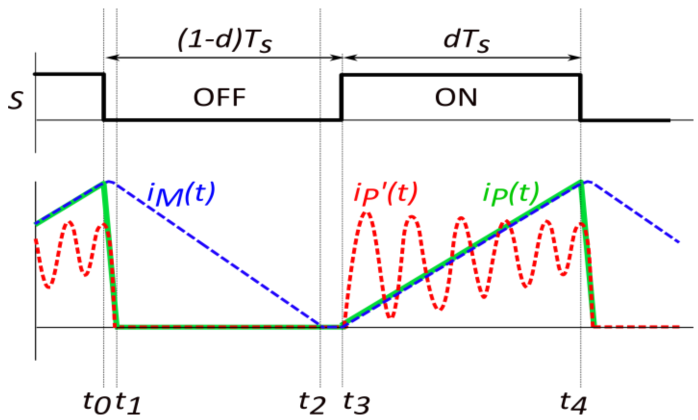

Fig. 4. Typical current response of a flyback converter

Interval 1 (t_0-t_1): Prior to the switching time t_0, the main switch *S* is in the *ON* state. When *S* is disconnected at $t = t_0$, the equivalent capacitance C_q is discharged by the magnetic inductance L_M. The resonance between C_q and L_M delays the energy transfer to the secondary winding until the C_q reaches $-V_o/N$ at $t = t_1$. Through C_{S_oss} and internal winding resistance, leakage inductance L_{lk}

simultaneously releases the energy it has been holding onto and creates the damped resonance. The current flowing in the magnetising inductance and losses created by leakage inductance at this interval can be expressed as:

$$i_{L_M}(t) = \frac{V_{in}}{Z_i}\sin(\omega_r t) + I_{LM\_t0}\cos(\omega_r t) \quad (3)$$

$$E_{L_{lk}} = \frac{1}{2}L_{lk}\left(I_{LM\_t0}\right)^2 \quad (4)$$

where $Z_i = \sqrt{L_M/C_q}$ and $\omega_r = 1/\sqrt{L_M C_{eq}}$. I_{LM_t0} is current flowing through L_M at switched off.

Interval 2 (t_1-t_2): At the moment when V_{Ceq} reached $-V_o/N$ at t_1, diode *D* at the secondary side of the converter turned on, allowing current from the magnetising inductor to flow through the output side. In this interval, the current I_{LM} starts decreasing and reaches zero at t_2. The decreasing current can be expressed by:

$$i_{L_M}(t) = -\frac{V_o}{NL_M}(t - t_1) + I_{LM_{t1}} \quad (5)$$

where V_o is the output voltage and I_{LM_t1} is current flowing through L_M at t_1.

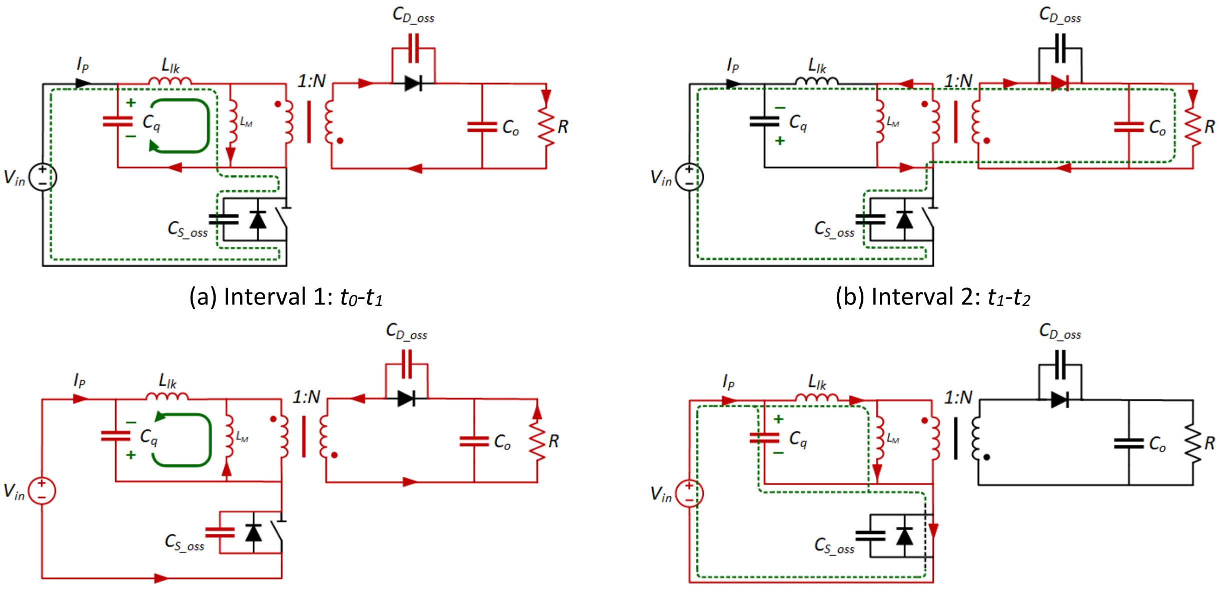

(a) Interval 1: t_0-t_1 (b) Interval 2: t_1-t_2

(c) Interval 1: t_2-t_3 (d) Interval 1: t_3-t_4

Fig. 5. Equivalent circuit for each interval inside switching cycle (a) t_0-t_1, (b) t_1-t_2, (c) t_2-t_3, and (d) t_3-t_4

Interval 3 (t_2-t_3): The capacitance and inductance, i.e., C_q, C_{S_oss}, C_{D_Oss}, L_M, *and* L_{lk}, formed the resonance circuit right after the L_M's energy has completely been transmitted to the converter's secondary side. At this instant, the initial voltage across the C_q changed its polarity, and the secondary side diode turned off when the current in L_M dropped to zero. However, at this particular moment, the voltage across the switch does not instantaneously decrease to zero. The interaction between L_M and C_q results in quasi-resonance, facilitating the attainment of zero V_{ds} at t_3. Therefore, the anti-parallel diode of the main switch *S* begins to conduct, ensuring zero voltage switching (ZVS) operation takes place. Magnetising current and equivalent capacitance-voltage at this interval are expressed as:

$$i_{L_M}(t) = -\frac{V_o}{NZ_i}\sin(\omega_r t) \tag{6}$$

$$v_{C_{eq}}(t) = -\frac{V_o}{N}\cos(\omega_r t) \tag{7}$$

This interval ends when V_{ceq} reaches V_{in} at t_3 and from Eq. (7), the following equation is deducted with $\vartheta = \omega_r t_3$:

$$\cos\vartheta = -\frac{NV_{in}}{V_o} \tag{8}$$

Further expansion of Eq. (8) results:

$$\vartheta = cos^{-1}\left(-\frac{1}{R}\right) \tag{9}$$

where R is the conversion ratio, $R = -V_o/NV_{in}$. From Eq. (9), it can be noted that the main switch, S of the converter can operate in ZVS with R is larger than 1.

Interval 4 (*t_3-t_4*): When S is switched on, the current builds up at leakage inductance L_{lk} and magnetising inductance L_M. Simultaneously, the damped resonance circuit formed by L_{lk}, C_q, and S charges the capacitance C_q to V_{in}. However, during the charging process, the input current I_p at the primary side consists of two resonance currents: the main charging current I_{p_charge} and the damped resonance current I_{p_res}. The main charging current is built up with the ω_{charge} influenced by L_M, C_q, C_{S_oss}, and C_{D_oss}. Employing a standard resonant circuit, the charging amplitude can be deducted as:

$$I_{p\_charge} = \frac{|V_o|\omega_{charge}C_{eq}}{N} \tag{10}$$

$$\omega_{charge} = \frac{1}{\sqrt{L_M \cdot C_{eq}}} \tag{11}$$

$$C_{eq} = C_q + C_{S\_oss} + N^2 C_{D\_oss} \tag{12}$$

On the other hand, the damped resonance current is generated with the ω_{res} influenced by L_{lk}, C_q, and C_{S_oss}. By means of the standard resonant circuit, the resonance current can be expressed as:

$$I_{p\_res} = \frac{|V_o|\omega_{res}(C_q + C_{S\_oss})}{N} \tag{13}$$

$$\omega_{res} = \frac{1}{\sqrt{L_{lk} \cdot (C_q + C_{S_{oss}})}} \tag{14}$$

4. Simulation and Experiment

Verification of the hypothesis and analysis of the influence of the transformer's parasitic element was executed by simulation and experimental work. MATLAB SIMULINK software was adopted for the simulation, and the experiment was carried out on the actual transformer. Physical measurements are made to determine the values of all the pertinent parameters that will be used in the simulation. The LCR-8000G programmable LCR meter is used on a Coilcraft NA5814-AL transformer in accordance with the prescribed procedure [26-28]. The measurement setup is shown in Figure 6(a). The inductance and AC resistance vs. frequency characteristic of the Device Under Test (DUT) is plotted in Figure 6(b). Magnetising inductance and AC resistance exhibit an increase in value as the frequency rises, while the value of leakage inductance decreases.

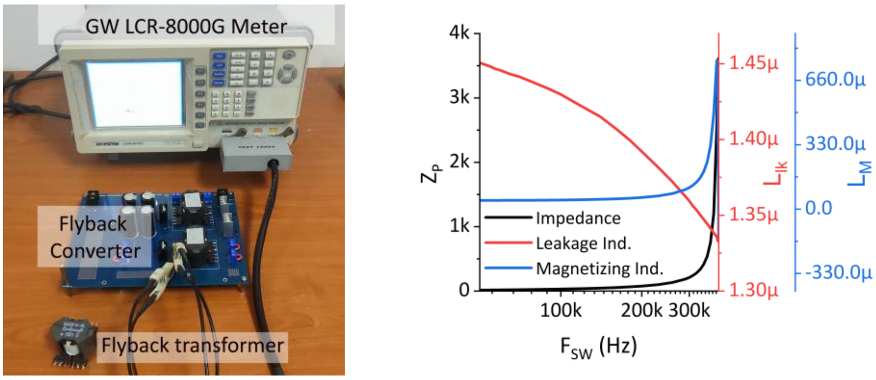

(a) (b)

Fig. 6. (a) Measurement setup of a 100W flyback transformer using an LCR meter. (b) Inductance and AC resistance vs. frequency characteristic

Table 1 displays the instantaneous parameters of the transformer that were examined at frequencies of 50 kHz, 160 kHz, and 200 kHz. It is interesting to note that the values change when the DUT is tested at different frequencies.

Table 1
Parameter of flyback transformer NA5814-AL at 50 kHz, 160 kHz, and 200 kHz

Parameter	50kHz	160kHz	200kHz	Unit
Primary inductance, *Lp*	50.06	-12.29**	-38.83	µH
Secondary inductance, *Ls*	1.65	-0.05436	-2.79	mH
Primary leakage inductance, *Likp*	1.33	1.44	1.35	µH
Magnetizing inductance, *Lm*	49.56	-13.73	-40.18	µH
Primary impedance, *Zp*	15.98	52.46	30.93	Ω
Primary capacitance, *Cp*	-198.7*	81.4	40.38	nF
Secondary capacitance, *Cs*	-6.15	18.2	2.49	nF

*The negative value of capacitance indicates the transformer behaves in inductive mode
**The negative value of inductance indicates the transformer behaves in capacitive mode

Figure 7 shows the waveform of the converter's primary current simulated with 50 kHz, 160 kHz, and 200 kHz switching frequencies. The simulation was executed on MATLAB SIMULINK simulation with key parameters listed in Table 1. It is important to note that the transformer used as DUT is designed to operate at 57 kHz, as claimed by its manufacturer [29]. Therefore, it is clearly seen from the simulation result that the primary current characteristic alters as the switching frequency shifts higher. Furthermore, based on the early measurements obtained, the data suggests that alterations in switching frequencies may lead to changes in the behaviour of transformer and converter operations. Parasitic elements from the surroundings, i.e., output capacitance of main switch, secondary diode, PCB stray capacitance, and inductance from cables, may also influence the overall characteristic of the transformer behaviour. Comparison with data depicted in Figure 6(b) indicates that the Self Frequency Resonance (SFR) is shifted to a lower value, from around 358 kHz to less than 160 kHz. Data from Table 1 shows evidence that the transformer is already in capacitive mode at 160 kHz.

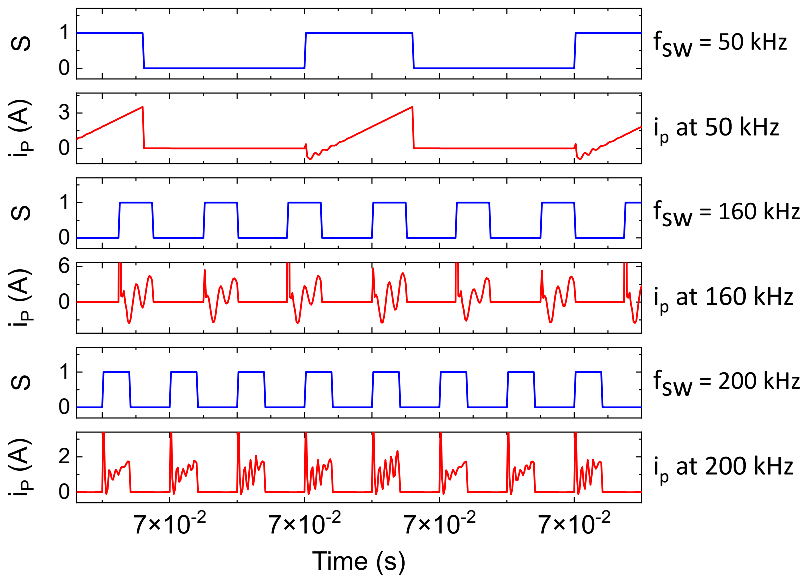

Fig. 7. MATLAB SIMULINK simulation converter's primary current i_P with diverse switching frequencies: 50 kHz, 160 kHz, and 200 kHz

Apart from simulation, experiments were conducted to verify the hypothesis and analysis of the parasitic element influence on the primary current of the converter at the higher switching frequency. Parameters of the experiment's main components are listed in Table 2, while the experimental setup is shown in Figure 8.

Table 2
Parameter of experimental circuit

Parameter	Type	Value
Flyback transformer, *T*	Coilcraft NA5814-AL	P_r : 100 W
Secondary diode, *D*	IDH06G65C6	V_r : 400V
Primary switch, *S*	UF3C065080T3S	V_{DS} : 650 V
Output capacitor, C_o	Electrolytic	960 µF
Load resistor, *R*	Aluminium-wire-wound	100 Ω 50 W

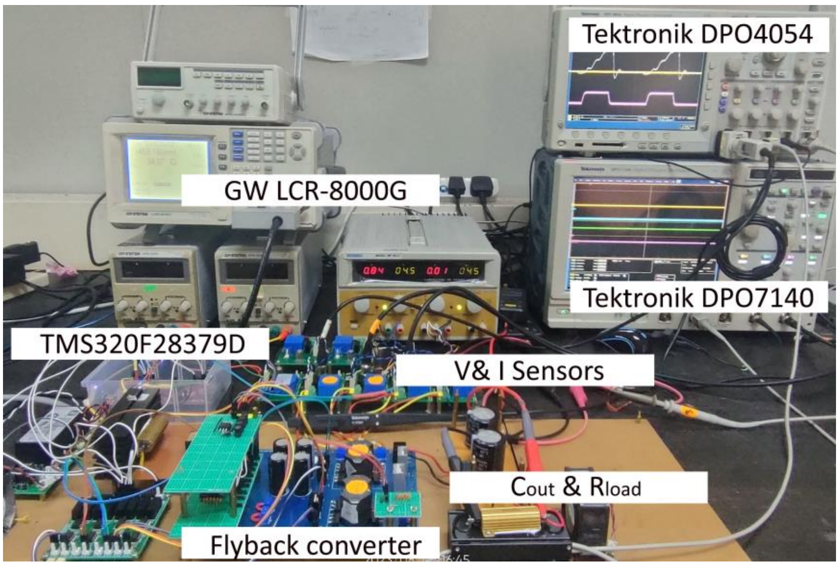

Fig. 8. Experiment setup

The results from the conducted experiment work are shown in Figure 9. Notably, a significant distortion occurs at the primary current during 160 kHz and 200 kHz switching frequencies, where a high-frequency oscillation starts as soon as *S* is turned on. On the other hand, the primary current shape is seen normal as long as the switching frequency is within the transformer's operational range, in this particular case, from 50 kHz to 60 kHz. As mentioned earlier in this article, the distorted primary current of the converter escalated a massive problem in the current peak control operation near the reference current's end. High-frequency oscillation might mistakenly trigger the main switch, e.g., the switching signal is toggled too soon before it is supposed to be. Consequently, the energy stored in L_m is less, resulting in poor efficiency to the overall converter's energy conversion.

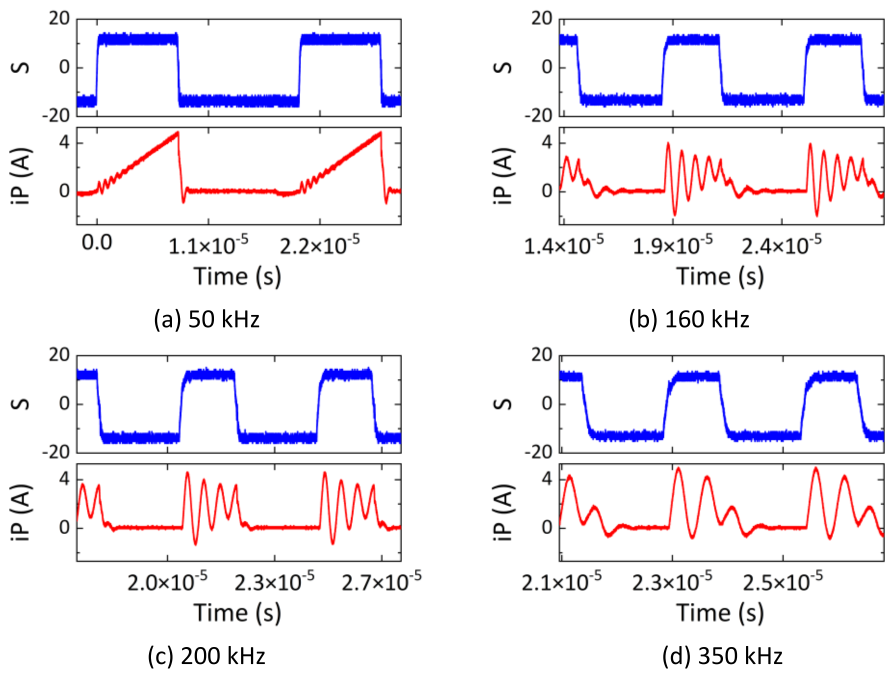

Fig. 9. Converter's primary current i_P with diverse switching frequencies: (a) 50 kHz, (b) 160 kHz, (c) 200 kHz, and (d) 350 kHz

5. Conclusion

This research extensively examines the impact of parasitic components on a DC-DC flyback converter. The simulation model is derived by starting with the equivalent circuit of the flyback transformer. The parasitic element's impact on the converter's primary current varies depending on the switching frequency. Previous data analysis indicated that the converter's characteristics and behaviour may change when the switching frequency is varied, particularly when it is increased to a greater value. The presence of parasitic elements in the transformer and other components in its vicinity is observed to cause distortion in the primary current. This distortion can lead to difficulties in specific applications, such as BCM's current peak control operation. The simulation results indicate that parasitic elements in the system lead to resonance and a significant distortion of the primary current in the converter, particularly during high frequency switching operations. Furthermore, the experimental findings obtained from the 100W flyback transformer exhibit a strong concurrence with the modelling and preliminary analysis conducted in this study, indicating that parasitic elements and the switching frequency play a significant role in determining the primary current characteristic of the converter. The analysis results and the findings from both modelling and experimental studies are expected to offer valuable insights for future research endeavours aimed at proactively mitigating the occurrence of resonance events.

Acknowledgement
The authors would like to acknowledge the Ministry of Higher Education for financial support via Fundamental Research Grant Scheme FRGS/1/2019/TK07/UPM/02/2. Also, a special thanks to Universiti Teknikal Malaysia Melaka and Universiti Putra Malaysia for their financial and technical support.

References

[1] Schmela, M. "SolarPower Europe (2020): Global market outlook for solar power 2020–2024." *Solar Power Eur., Rue d'Arlon* (2020): 69-71.
[2] International Energy Agency. "Renewable Energy Market Update: Outlook for 2022 and 2023." *OECD Publishing*, (2022).
[3] Abdelilah, Yasmina, Heymi Bahar, Trevor Criswell, Piotr Bojek, François Briens, and P. L. Feuvre. "Renewables 2020: Analysis and Forecast to 2025." *IEA: Paris, France* (2020).
[4] Yaakub, Muhamad Faizal, Mohd Amran Mohd Radzi, Faridah Hanim Mohd Noh, and Maaspaliza Azri. "Silicon carbide power device characteristics, applications and challenges: an overview." *International Journal of Power Electronics and Drive Systems* 11, no. 4 (2020): 2194. https://doi.org/10.11591/ijpeds.v11.i4.pp2194-2202
[5] Kumar, Ch Santosh, and S. Tara Kalyani. "Improvement of Power Quality Using Reduced Switch Count Eleven-Level Inverter in Smart Grid." *Journal of Advanced Research in Applied Sciences and Engineering Technology* 31, no. 1 (2023): 14-33. https://doi.org/10.37934/araset.31.1.1433
[6] Ma, Raja Noor Farah Azura Raja, Nur Amira Syahirah Azmar, Mohd Syahriman Mohd Azmi, Nor Suriya Abd Karim, Nor Hafizah Md Husin, Norhisam Misron, and Nida Sri Utami. "Sustainable Urban Planning: Criteria for Efficient Photovoltaic Electric Vehicle Charging Stations Deployment in Malaysia." *Semarak International Journal of Electronic System Engineering* 1, no. 1 (2024): 35-45. https://doi.org/10.37934/ard.111.1.18
[7] Rababah, Haitham Esam, Azhar Ghazali, Mohd Hafizal Mohd Isa, Zalena Abdul Aziz, and Mohamed HS Shaat. "Sustainable Urban Energy Solutions: Investigating the Solar Potential of Vertical Façades Amidst Adjacent Buildings in Kuala Lumpur, Malaysia." *Journal of Advanced Research in Applied Sciences and Engineering Technology* 32, no. 3 (2023): 488-505. https://doi.org/10.37934/araset.32.3.488505
[8] Jiménez-Martínez, Jacinto M., Esther de Jódar, and José Villarejo. "Parasitic Capacitance Effects on Active Clamp Flyback Output Characteristics: Application to IPOP Connection." *Energies* 15, no. 9 (2022): 3201. https://doi.org/10.3390/en15093201
[9] Srinivasan, Mahesh. "Analysis and stabilization of CCM flyback converters supplying constant power loads." In *2021 IEEE Kansas Power and Energy Conference (KPEC)*, pp. 1-6. IEEE, 2021. https://doi.org/10.1109/KPEC51835.2021.9446229
[10] Lodh, Tirthasarathi, Nataraj Pragallapati, and Vivek Agarwal. "Novel control scheme for an interleaved flyback converter based solar PV microinverter to achieve high efficiency." *IEEE Transactions on industry applications* 54, no. 4 (2018): 3473-3482. https://doi.org/10.1109/TIA.2018.2818655
[11] Zhang, Feng, Yunxiang Xie, Yanshen Hu, Gang Chen, and Xuemei Wang. "A hybrid boost–flyback/flyback microinverter for photovoltaic applications." *IEEE Transactions on Industrial Electronics* 67, no. 1 (2019): 308-318. https://doi.org/10.1109/TIE.2019.2897543
[12] Wang, Shuo, and Fred C. Lee. "Analysis and applications of parasitic capacitance cancellation techniques for EMI suppression." *IEEE Transactions on Industrial Electronics* 57, no. 9 (2009): 3109-3117. https://doi.org/10.1109/TIE.2009.2038333
[13] Balbayev, Gani, Arailym Nussibaliyeva, Baurzhan Tultaev, Erlan Dzhunusbekov, Gulsara Yestemessova, and Aliya Yelemanova. "A novel regenerative snubber circuit for flyback topology converters." *Journal of Vibroengineering* 22, no. 4 (2020): 983-992. https://doi.org/10.21595/jve.2020.20898
[14] Tanrıkulu, Umit, Erdem Akboy, and Burak Akın. "Design And Analysis Of A Flyback Converter With Improved Snubber Cells." *Sigma Journal of Engineering and Natural Sciences* 38, no. 4 (2020): 2205-2216.
[15] Prieto, M. J., Alicia Fernández, J. M. Diaz, J. M. Lopera, and J. Sebastian. "Influence of transformer parasitics in low-power applications." In *APEC'99. Fourteenth Annual Applied Power Electronics Conference and Exposition. 1999 Conference Proceedings (Cat. No. 99CH36285)*, vol. 2, pp. 1175-1180. IEEE, 1999. https://doi.org/10.1109/APEC.1999.750517

[16] Das, Annoy Kumar, and Baylon G. Fernandes. "Study of frequency-dependent parasitics' effects on resonance frequencies of a two-winding medium/high-frequency transformer." In *2020 IEEE International Conference on Power Electronics, Drives and Energy Systems (PEDES)*, pp. 1-6. IEEE, 2020. https://doi.org/10.1109/PEDES49360.2020.9379780
[17] Mendivil, H. C., and LJ C. Ruíz. "Analysis of the high gain DC-DC converters including parasitic elements in photovoltaic systems." In *2020 IEEE International Autumn Meeting on Power, Electronics and Computing (ROPEC)*, vol. 4, pp. 1-6. IEEE, 2020. https://doi.org/10.1109/ROPEC50909.2020.9258704
[18] Li, Min, Bo Zhang, and Dongyuan Qiu. "Sneak circuit analysis for a DCM flyback DC-DC converter considering parasitic parameters." In *2016 IEEE 8th International Power Electronics and Motion Control Conference (IPEMC-ECCE Asia)*, pp. 1151-1155. IEEE, 2016.
[19] Kewei, Huang, Li Jie, Hu Xiaolin, and Fan Ningjun. "Analysis and simulation of the influence of transformer parasitics to low power high voltage output flyback converter." In *2008 IEEE International Symposium on Industrial Electronics*, pp. 305-310. IEEE, 2008. https://doi.org/10.1109/ISIE.2008.4676953
[20] Gao, Mingzhi, Min Chen, Chi Zhang, and Zhaoming Qian. "Analysis and implementation of an improved flyback inverter for photovoltaic AC module applications." *IEEE transactions on Power Electronics* 29, no. 7 (2013): 3428-3444. https://doi.org/10.1109/TPEL.2013.2279266
[21] Nanakos, Anastasios Ch, Georgios C. Christidis, and Emmanuel C. Tatakis. "Weighted efficiency optimization of flyback microinverter under improved boundary conduction mode (i-BCM)." *IEEE Transactions on Power Electronics* 30, no. 10 (2014): 5548-5564. https://doi.org/10.1109/TPEL.2014.2372005
[22] Jagpal, Lovejeet Singh. "Study of effect of Parasitic on Conducted Emissions from Flyback Converter through Simulation." In *2018 15th International Conference on ElectroMagnetic Interference & Compatibility (INCEMIC)*, pp. 1-4. IEEE, 2018. https://doi.org/10.1109/INCEMIC.2018.8704552
[23] Spiazzi, Giorgio, Paolo Mattavelli, and A. Costabeber. "Effect of parasitic components in the integrated boost-flyback high step-up converter." In *2009 35th Annual Conference of IEEE Industrial Electronics*, pp. 420-425. IEEE, 2009. https://doi.org/10.1109/IECON.2009.5414959
[24] Li, Yiming, Shuo Wang, Honggang Shen, and Srikanth Lakshmikanthan. "Inductor Winding Capacitance Cancellation for Flyback Converters without Grounding Paths." In *2020 IEEE International Symposium on Electromagnetic Compatibility & Signal/Power Integrity (EMCSI)*, pp. 640-645. IEEE, 2020. https://doi.org/10.1109/EMCSI38923.2020.9191583
[25] Leuenberger, David, and Jürgen Biela. "Accurate and computationally efficient modeling of flyback transformer parasitics and their influence on converter losses." In *2015 17th European Conference on Power Electronics and Applications (EPE'15 ECCE-Europe)*, pp. 1-10. IEEE, 2015. https://doi.org/10.1109/EPE.2015.7309194
[26] Desk. https://bkprecision.my.site.com/desk/s/article/how-to-use-a-lcr-meter
[27] Stauffer, Lee. "Cv measurement tips, tricks, and traps." *Keithley Instruments, Inc* 3109 (2008): 1-14.
[28] Tegam. "LCR Meter Measurement Accuracy - Tegam." *Application Note 301*, (2015). https://www.tegam.com/wp-content/uploads/2015/10/AN301.pdf
[29] Coilcraft. "NA5814, NA5919 Flyback Transformer for Microchip Microinverter AN1444." *Coilcraft*. https://www.coilcraft.com/en-us/products/transformers/power-transformers/power-converter-transformers/na5814